Spin and Charge Memory Retention in Localized Spin-Orbit Coupled Systems

A Thesis

submitted to
Indian Institute of Science Education and Research Pune
in partial fulfillment of the requirements for the
BS-MS Dual Degree Programme

by

Aditya Chincholi

Indian Institute of Science Education and Research Pune
Dr. Homi Bhabha Road,
Pashan, Pune 411008, INDIA.

April, 2023

Supervisor: Dr Rajdeep Sensarma

Certificate

This is to certify that this dissertation entitled Spin and Charge Memory Retention in Localized Spin-Orbit Coupled Systems towards the partial fulfilment of the BS-MS dual degree programme at the Indian Institute of Science Education and Research, Pune represents study/work carried out by Aditya Chincholi at Tata Institute of Fundamental Research, Mumbai under the supervision of Dr Rajdeep Sensarma, Associate Professor, Department of Physics , during the academic year 2022-2023.

Dr Rajdeep Sensarma

Committee:

Dr Rajdeep Sensarma

Dr Sreejith G J

Declaration

I hereby declare that the matter embodied in the report entitled Spin and Charge Memory Retention in Localized Spin-Orbit Coupled Systems are the results of the work carried out by me at the Department of Physics, Indian Institute of Science Education and Research, Pune, under the supervision of Dr Rajdeep Sensarma and the same has not been submitted elsewhere for any other degree.

Aditya Chincholi

Acknowledgments

I'm extremely grateful to my supervisor Dr Rajdeep Sensarma and my PhD mentor Mursalin Islam for guiding me in this work. I'd like to thank my family for their utmost support during this time. I'd like to express my gratitude to Tata Institute of Fundamental Research, Mumbai for providing the computational resources that made this work possible. I'm grateful to Dr Sreejith G J without whose guidance and support this would not have been possible. This work would also not have been possible without the support of Prajakta Umbarkar, Goirik Chakrabarty, Anuja Raorane, Abhishek Ravishankar and Purva Parmar. I'm thankful to the Kishore Vaigyanik Protsahan Yojana scholarship for enabling me to pursue this project.

Abstract

We investigate the non-interacting 2D Anderson model with Rashba type spin-orbit coupling over the localized-delocalized phase transition. We calculate a coarse-grained picture of the disorder strength - SOC coupling strength phase diagram. We also investigate the persistence of information about the initial state through imbalance measurements. We compare the imbalance retention for different densities such as charge density, S_i for different initial conditions. We show that the charge and spin imbalances behave in qualitatively different ways as we move through the parameter space. The spin imbalance is less robust than the charge imbalance for small spin-orbit coupling but more robust at large coupling values. The dependence of the charge imbalance on the presence/absence of a spin pattern in the initial condition is also investigated.

Contents

List of Figures

Chapter 1

Introduction

Classical and quantum systems show quite different contrasting behaviour in response to potential landscapes. Classical systems can localize a particle within a region of space only if the energy of the particle is lower than the height of the potential barrier surrounding the particle. However, quantum systems display tunnelling which in typical systems disallows a particle to be restricted by a finite potential barrier. Any particle that is blocked by a finite potential barrier will tunnel to the other side of the barrier. The amplitude of the wavefunction decreases exponentially with the width of the barrier but the wavefunction is non-zero in the region beyond the barrier and the amplitude does not decrease beyond the width of the barrier if the potential outside is flat. This means that a quantum particle in a finite potential well has a non-zero chance of "escaping" to beyond the well irrespective of the height and width of the potential, as long as they are finite. However, Anderson localization is a phenomenon that allows a quantum system to localize a particle within a small region despite the potential landscape being finite and the barrier not being higher than the particle's energy [2].

A disordered potential, simply called disorder, is a potential field whose values are random. In practical systems, disorder is the result of impurity, imperfections and other defects in the sample. Since all samples that can be prepared inevitably contain such factors, most samples that can be produced in a lab will have some degree of disorder. The presence of disorder in the system leads to significant effects on the system dynamics and usually cannot be be neglected or ignored. These effects can be non-perturbative and hence require careful

consideration. Anderson localization is one such effect which we study in this work.

The Anderson localization effect happens in systems with sufficiently large disorder in the potential. The presence of a disordered potential, a potential whose values are drawn randomly from a distribution, can localize a particle within a small region of space [2]. The kinetic energy of the particle need not be smaller than the average height of the potential surrounding the particle. The effect occurs due to the presence of multiple, coherent scatterers leading to an exponentially decreasing probability of the particle being transmitted across the sample.

Since disorder is found in most practical systems and coherent scattering requires waves which are also ubiquitous in nature, the phenomenon can be seen in various systems. It can be seen in light waves in diffusive media [34, 32], photonic crystals [30], [7] and atomic matter waves in a cold atom systems [24, 5, 28].

This localization has consequences for the transport properties of the particle in that medium. Most notably, a strongly localized system will act as an insulator while a delocalized system will act as a metallic conductor. So the effect gives rise to a metal-insulator transition that shows localized behaviour for strong disorder and delocalized behaviour for weak disorder in certain systems.

In typical quantum systems, most of the eigenstates are delocalized. These have support over a significant portion of the Hilbert space. Any initial state with a a positional structure will evolve as independent, delocalized eigenstates leading to the delocalization of the particles over time. Typically, this final state would be a thermal state of the system. As a result, the positional information about the initial state would be lost as the system evolves. This process of erasure of the information about the initial conditions at the macroscopic scale is thermalization. If the system is integrable, the initial state could be reconstructed using the conserved quantities measured at later times. However, typical quantum systems are non-integrable and thus, we are usually unable to get any information about the structure of the initial state.

In contrast, disordered systems displaying localization also exhibit dynamics that may not lead to a thermal state. Starting from an initial particle configuration, localized systems have been shown to retain the information about the spatial pattern of the particles in the initial state whereas this memory is lost in delocalized systems [8]. As a result, disordered

systems show interesting qualities that allow them to retain the information about the initial state. This robust persistence of memory of the initial states make them good candidates for preserving spatial patterns in the system states that may be important for a sample for other effects and experiments.

Systems with interactions that show localization are an important category of systems as they exhibit non-equilibrium dynamics since they may not thermalize when starting from certain initial states. Adding interactions can lead to delocalization in systems that otherwise show localization. Therefore, localized interacting systems are special and are categorized differently than their non-interacting counterparts. This phenomenon is called Many-Body Localization and is a topic of intense study. In this work, however, we consider only systems without interaction.

Spin-orbit coupling in condensed matter systems is an interaction between the spin of a particle and the magnetic field induced by its motion. This coupling, therefore, makes the particle motion spin-dependent by connecting the spin of the particle to its orbital motion. Adding spin orbit coupling to the 2D Anderson model leads to the appearance of a metal-insulator transition in this system since the spin-orbit coupling in general causes a delocalizing effect on the particles. [13] This phase transition now occurs in a 2D parameter space since the disorder strength and the spin-orbit coupling strength are now both factors that affect the localization effect.

The addition of spin-orbit coupling breaks the conservation of spin i.e the spin rotational symmetry and allows for a richer dynamics to come into play in our systems since now the spin density and the charge density both show localization. This is in contrast to systems without spin interactions where only the charge density shows localization. By adding spin-orbit coupling to the system, we can now probe the relationship between the memory of the initial spin patterns and the initial charge patterns. We show in our work that the two show qualitatively different behaviour in the presence of spin-orbit coupling and that they are independent of the other.

The difference in the behaviour spin and charge memory retention in such systems may be important in creating procedures that need to create and maintain particular spin and charge patterns in a 2D system. One key motivation to study the effects of spin and charge patterns would be to see if the presence of one of spin or charge patterns could give rise to a pattern in another quantity or play a significant role in the decay of the information about

this quantity. Since disorder is ubiquitous, these results would form the foundation for any further work that may focus on similar systems with added interactions.

The setups described in this work may be experimentally realized through cold atom experiments. Recent experimental work has enabled construction of spin-orbit coupled cold atomic systems in optical lattices [20]. Huang et al have shown experimental realizations of 2D spin-orbit coupled Fermi gases [18] and theoretically 2D Anderson transitions have been studied for cold atoms in speckle potentials [27, 35]. Therefore, they provide the possibility of an experimental verification of our results.

Chapter 2

Localization in Disordered Quantum Systems

2.1 Localization

We define localization of a particle at point x as the wavefunction of a particle that shows amplitudes which decay at least exponentially with the peak at x. The main question is that if we start with an initial state where the particle is present at x, will the wavefunction remain localized at the point x at long times?

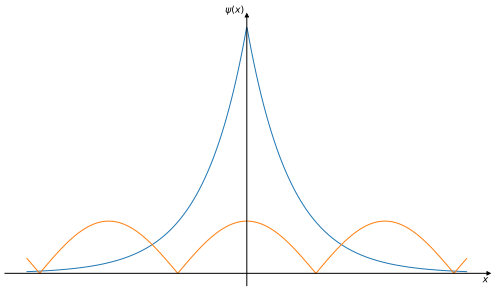

Figure 2.1: Example of a localized (blue) and a delocalized state (orange).

The characteristic length scale of the exponential decay is called the localization length. In practice, the localization of a state can be quantified using various quantities which may

be easier to measure. The localization length is one such quantity, but it is often hard to measure directly and is often inferred from other quantities or by fitting.

One way to quantify localization is in terms of Inverse Participation Ratio (IPR). IPR is defined as

$$IPR[\psi(x)] = \sum_x |\psi(x)|^4 \tag{2.1}$$

For a delocalized state, the IPR scales with the system size L as $1/L$. For a localized state, the IPR remains nearly constant with the system size. This allows us to distinguish between states by computing them for different system sizes. Since it involves matching states for different system sizes, we have not adopted this approach in our work.

The localization length can be found by calculating the Green's function of the system and using the fact that the Green's function squares will decay exponentially with distance over length scales corresponding to the localization length. We use this in the first part of our work.

The localization length can also be found from the long time imbalance of certain quantities like particle and spin densities in the system. This is discussed in Chapter 4.

2.2 Anderson Localization

The Anderson model is one of the simplest examples of systems showing localization. The model, introduced by P. W. Anderson [2], is given by

$$H = \sum_i \epsilon_i c_i^\dagger c_i - t \sum_{\langle ij \rangle} c_i^\dagger c_j \tag{2.2}$$

where t is the hopping strength, ϵ_i are random onsite potentials (known as disorder) drawn from a uniform distribution $[-W/2, W/2]$ and W is called the disorder strength.

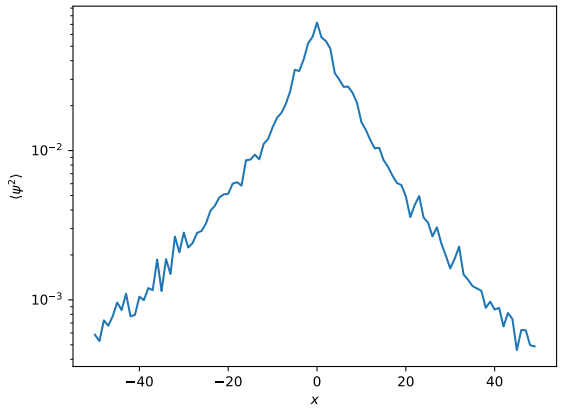

Figure 2.2: $\langle\psi^2\rangle$ for the 1D Anderson model starting from initial state of a Gaussian wavepacket at $W = 3$ over 100 disorder realizations and after $t = 100$

In the absence of disorder, the Anderson model is a tight-binding model whose solutions are plane waves. In 1D, the model shows localization at any non-zero disorder strength W. The model has been studied extensively since it was proposed by Anderson in 1958. The localization length is comparable to the mean free path length scale. [33]

In 2D on a square lattice, the model still remains localized for any non-zero disorder [1] [12]. However, the localization effect is much weaker in the sense that, the localization length ξ can be very large, especially for weak disorder. ξ can often exceed the size of finite size systems, which leads to the system appearing delocalized in simulations even though it is not in the infinite size limit. The $d = 2$ case is the lower critical dimension for the Anderson transition which is visible in higher dimensions.

In 3D cubic lattice, the system shows a phase transition between the system being localized and the system being delocalized as the disorder strength is varied. [2] This is known as the Anderson Metal-Insulator transition. The system shows delocalization, thus behaving as a metal, for weak disorder ($W < W_c$) and localization with insulator characteristics for strong disorder ($W > W_c$).

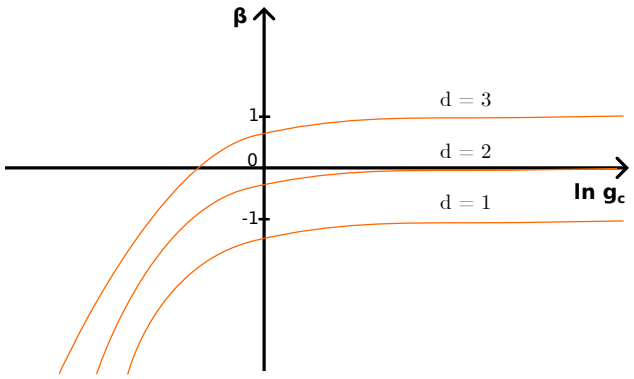

Figure 2.3: Schematic plot of β-function

2.3 Scaling Theory

One way to understand the Anderson phase transtion is via scaling theory introduced by Abrahams et al [1]. For a d-dimensional metallic sample of side length L, the conductance $g(L)$ scales as L^{d-2} in the classical (Drude) limit. We define the β-function as

$$\beta(g) := L\frac{d}{dL}\ln g(L) = \frac{d\ln g(L)}{d\ln(L/L_0)} \tag{2.3}$$

$$= d-2 \text{ (to leading order)} \tag{2.4}$$

This is also known as the "renormalization flow". When the β-function is negative, the conductance decreases with L, so it represents an insulating phase. On the other hand, a positive β-function represents a conducting phase as the conductance increases with L.

For $d = 1$, the β-function is always negative and $\lim_{g\to\infty}\beta(g) = -1$. Therefore, the system is always localized and insulating. For $d = 2$, the function is still negative, but the asymptotic value is zero. Therefore, we need further correction terms to understand whether the system admits a transition or not. It turns out that the β-function is always negative and the asymptotic value is zero because of "Weak Localization" corrections.

$$\beta(g) = d-2-\frac{c_d}{g}+O(g^{-2}) \tag{2.5}$$

where a microscopic calculation is needed to find the value of the coefficient c_d (which is dimension dependent).

For the 2D case, we can integrate out the expression to get $g(L) = g_0 - c_2 \ln L/L_0$. Taking $L_0 = l$, where l is the mean free path, we have $g_0 = g(L_0) \gg 1$ since conduction is ballistic at that length scale. The localization length can be found by using $g(\xi_{loc}) = O(1)$ as this is where the transition to strong localization would occur. Therefore, we get $\xi_{loc} \sim lexp(g_0/c_2)$. Scaling theory, with correction terms, thus predicts that all states are localized in 2D even for small disorder. However, this is a very large localization length as $c_2 = O(1)$. Experimentally achieving reasonable values for localization is challenging.

For $d = 3$, the β-function, crosses over from negative to positive and the point of crossing indicates the phase transition. The derivative of the β-function at the critical point also gives us the critical exponent of the transition. On the insulator side, the localization length ξ_{loc} diverges as $(W - W_c)^{-\nu}$ where $\nu = 1/[d\beta/dg]_{g_c}$. On the metallic side, the $\beta > 0$ branch of the renormalization flow gives us $D \propto (W_c - W)^{\nu}$ for the diffusion constant D.

2.4 Weak Localization

In 2D, the scaling theory of localization requires a correction term to predict the resultant effect as $d = 2$ forms the lower critical dimension for the transition. In the 2D Anderson model, the phenomenon of Weak Localization results in the presence of localization even at arbitrarily low disorders. However, the localization length in these cases can be extremely large and can easily exceed the system size in finite size systems. [1].

Weak localization is a constructive interference effect that increases the probability of a particle to return to it's original site. In order to calculate this effect, we need to do a microscopic calculation for the intensity transport averaged over an ensemble of disorder instances.

We can calculate this by considering perturbative corrections wherein each site is considered a scatterer due to its disorder potential.

First, we consider the Bethe-Salpeter equation for the intensity propogator $\Phi = \langle G^R G^A \rangle$

$$\Phi = \langle G^R \rangle \langle G^A \rangle + \langle G^R \rangle \langle G^A \rangle U \Phi \tag{2.6}$$

where U is the intensity scattering operator and depends on the details of the disorder.

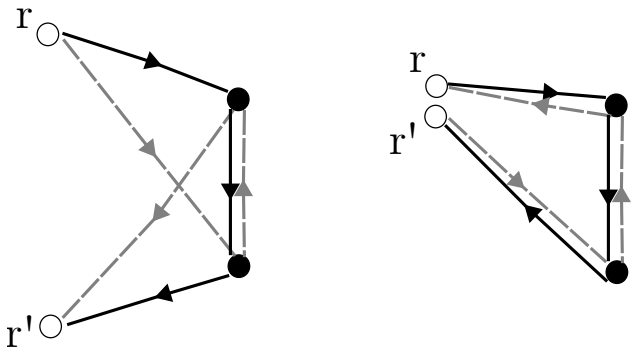

Figure 2.4: Crossed Diagram

The contributions to U come from the diffusion scattering along with the weak localization corrections. The leading order terms come from the classical, incoherent scattering process which leads to diffusive behaviour. The corrections terms can be calculated by considering the coherent scattering processes which involve an intermediate propogation between site r and r' as shown in Figure 2.4. The first type of correction terms we can consider are the diagrams with two crossed lines. The two lines are time-reversed counterparts. Usually, the phase difference between the ψ and ψ^* amplitudes is large and the contributions average to nearly zero when we do an ensemble average. However, the Weak Localization corrections correspond to closed loop diagrams where $r = r'$. There is no phase difference between a closed loop and its time-reversed counterpart, leading to constructive interference which enhances the backscattering probability. This is true irrespective of the number of scatterers along the loop path. Therefore, our weak localization correction consists of all the maximally crossed diagrams.

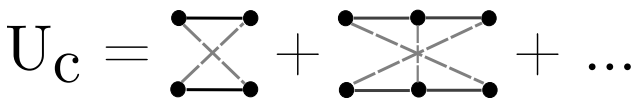

Figure 2.5: Cooperon Contribution

This Cooperon correction term enhances the probability of the particle returning to it's

original location. Overall, this correction term leads to the 2D Anderson model showing localization even for small disorder, even though the localization length may be large.

Chapter 3

Spin-Orbit Coupled Anderson Model

3.1 Spin-Orbit Coupling

Spin-orbit coupling involves the kinetic degrees of freedom of a particle influencing and being influenced by the direction of its intrinsic spin magnetic moment. It is found to be ubiquitous in nature. Although the origin of spin-orbit coupling is relativistic, the strength and form of the coupling are strongly dependent on the material and the lattice environment in which the particle resides [23]. The effect of spin-orbit coupling tends to be larger in heavier elements [31]. The lack of inversion symmetry in a material is known to further enhance the effect of spin-orbit coupling exhibited by the material [15]. In fact, researchers have tried to engineer systems with strong spin-orbit coupling by constructiing heterostructres of materials [11].

Spin-orbit coupling is an essential part of many interesting systems in modern condensed matter topics such as spintronics [36], topological insulators [16] and heterostructres hosting exotic Majorana modes [22], which can be useful in topological quantum computing. It is also an important ingredient for observing magnetic skyrmions [25] and for use in modern racetrack memories [6]. Since practical material samples always have intrinsic disorder, it is important to study the effects of disorder, particularly the physics of localization, in the presence of spin-orbit coupling.

In 2D, a system of fermions with disorder on a square lattice with local nearest neighbour hopping is always localized but with an extremely large localization length for weak disorder

[1]. In 3D, such a system exhibits a phase transition from a partially localized phase with a mobility edge to a completely localized phase [2]. In the presence of spin-orbit coupling, however, the same transition can now be seen in 2D. This can be seen from scaling theory, originally introduced by Abrahams et al, due to the effect of weak anti-localization [13, 17].

The presence of spin-orbit coupling in a disordered system opens up new pathways for the particle to move as the spin can now hop to a neighbouring lattice site in two ways, one which conserves the spin and one which involves a spin flip. Since localization occurs due to a coherent interference of return probability amplitudes, the addition of spin-orbit coupling changes the localization behaviour of the system. The spin-orbit coupling breaks the spin symmetry of the system and the spin of the particle is no longer a conserved quantity. The time-reversed analog of a closed path now has different spins as spins flip under time-reversal. Therefore, the interference is destructive, leading to Weak Anti-Localization. As a result, the system now exhibits two competing parameters, the disorder strength (W) which increases the tendency to localize as W increases and the spin-orbit coupling strength (α) which increases the tendency of the system to delocalize.

This richer dynamics introduced by the spin-orbit coupling into the system leads to questions surrounding the localization behaviours of the spin and charge densities in such systems. We can ask whether the localization lengths for the two are the same and if they show different behaviours as W and α are varied. We expect the spin and charge densities to delocalize at large spin-orbit coupling strengths. At low values of spin-orbit coupling strength, we expect both the charge and spin to be localized but they could show differences in their behaviour as the disorder strength and spin-orbit coupling strength are varied. This difference in localization behaviour can have implications for the spin and charge transport in the system since localization will suppress the conductance of the spin/charge in the system. Having different localization lengths and behaviours over the parameter space would lead to interesting consequences as they may show transport at different rates.

3.2 Model

We work with spin 1/2 fermions on a 2D square lattice governed by a tight-binding hamiltonian with nearest neighbour hopping, random onsite potentials and Rashba type spin-orbit coupling. Open boundary conditions are used. The hamiltonian for this system is given by

Eq 3.1:

$$H = \sum_{i,\sigma} \epsilon_i c^\dagger_{i,\sigma} c_{i,\sigma} - t \sum_{\langle ij \rangle,\sigma} c^\dagger_{i,\sigma} c_{j,\sigma} + \alpha \sum_{\langle ij \rangle,\sigma} V^{\sigma,-\sigma}_{ij} c^\dagger_{i,\sigma} c_{j,-\sigma} \tag{3.1}$$

$$\begin{aligned} H_{soc} &= \alpha \sum_{\langle ij \rangle,\sigma} V^{\sigma,-\sigma}_{ij} c^\dagger_{i,\sigma} c_{j,-\sigma} \\ &= \alpha \Big[c^\dagger_{(x-1,y),\uparrow} c_{(x,y),\downarrow} - c^\dagger_{(x+1,y),\uparrow} c_{(x,y),\downarrow} - i c^\dagger_{(x,y-1),\uparrow} c_{(x,y),\downarrow} + i c^\dagger_{(x,y+1),\uparrow} c_{(x,y),\downarrow} \\ &\quad - c^\dagger_{(x-1,y),\downarrow} c_{(x,y),\uparrow} + c^\dagger_{(x+1,y),\downarrow} c_{(x,y),\uparrow} - i c^\dagger_{(x,y-1),\downarrow} c_{(x,y),\uparrow} + i c^\dagger_{(x,y+1),\downarrow} c_{(x,y),\uparrow} \Big] \end{aligned} \tag{3.2}$$

Each onsite potential ϵ_i is drawn from a uniform random distribution $\epsilon_i \in [-W/2, W/2]$. The hopping is restricted to nearest neighbour sites with a strength t which we set to unity for the remainder of this work. The spin-orbit coupling, with strength α, is restricted to nearest neighbour terms only and is expanded in Eq 3.2. A schematic for the spin-orbit coupling is shown in Figure 3.1.

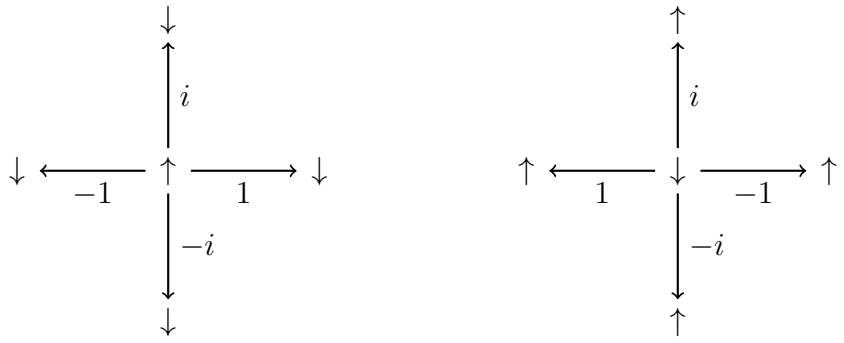

Figure 3.1: Coefficients for the nearest neighbour spin-orbit coupling phases $V^{\alpha\beta}_{ij}$.

This system has been studied previously in literature. Evangelou et al showed that there exists a metal-insulator transition in this system [13]. The exponent for this transition has been calculated to increasing degrees of precision to $\nu = 2.73 \pm 0.02$ by several authors [13, 3, 14, 4]. Here ν is the critical exponent which describes the divergence of the localization length $\xi_{loc} \sim (W - W_c)^{-\nu}$. Fastenrath et al have studied the phase diagram of the transition numerically. Their calculations, however, are limited to a maximum system size of $L = 20$ and their data points lie on selective planes of the parameter space. They calculated the

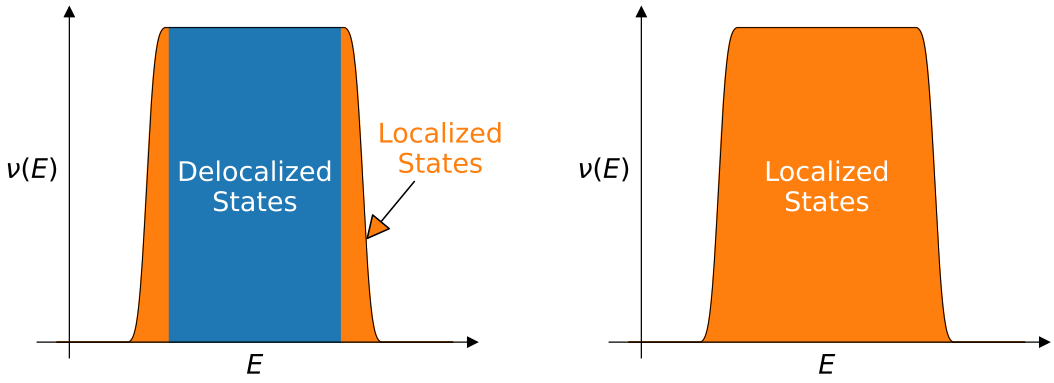

(a) Delocalized Phase

(b) Localized Phase

Figure 3.2: Schematic Diagram of Density of States before and after transition.

phase diagram in $W - \alpha$ for $E = 0$ on a maximum system size of $L = 20$ with a transfer matrix calculation over a limited number of data points and the phase diagram in the $E - W$ plane was calculated for a particular value of spin-orbit coupling strength $\alpha = 1$. This was done by looking at the intersection of $1/\xi_{ren}(E)$, where ξ_{ren} is the renormalized localization length, curves for different system sizes $L = 4$ to $L = 16$ computed through a transfer matrix approach. This gives us a very limited picture of the phase diagram and is also limited to small system sizes. Therefore, we have attempted to analyze it by a different method.

While energy-dependent localization lengths of this system are beyond the scope of this thesis, the above mentioned studies allow us to visualize the spectral structure in ways that help us understand some of the results ahead. The localization lengths $\xi_{\alpha\beta}$ can be extracted from each eigenstate individually giving rise to a localization length $\xi_{\alpha\beta}(E)$ as a function of energy. This function shows a mobility edge in the spectrum which separates the localized eigenstates and delocalized eigenstates. In the delocalized phase, the spectrum has a mobility edge which separates the eigenstates into delocalized states in the bulk of the spectrum and localized states near the edge of the spectrum. As the system moves to the localized phase, the mobility edges move towards the centre and vanish at the phase transition with all the eigenstates being localized [14]. We can see this in the schematic diagram of the density of states in Figure 3.2.

We attempt to calculate an overall picture of the phase space formed by the disorder strength and the spin-orbit coupling strength for the whole system. For each (W, α), we create

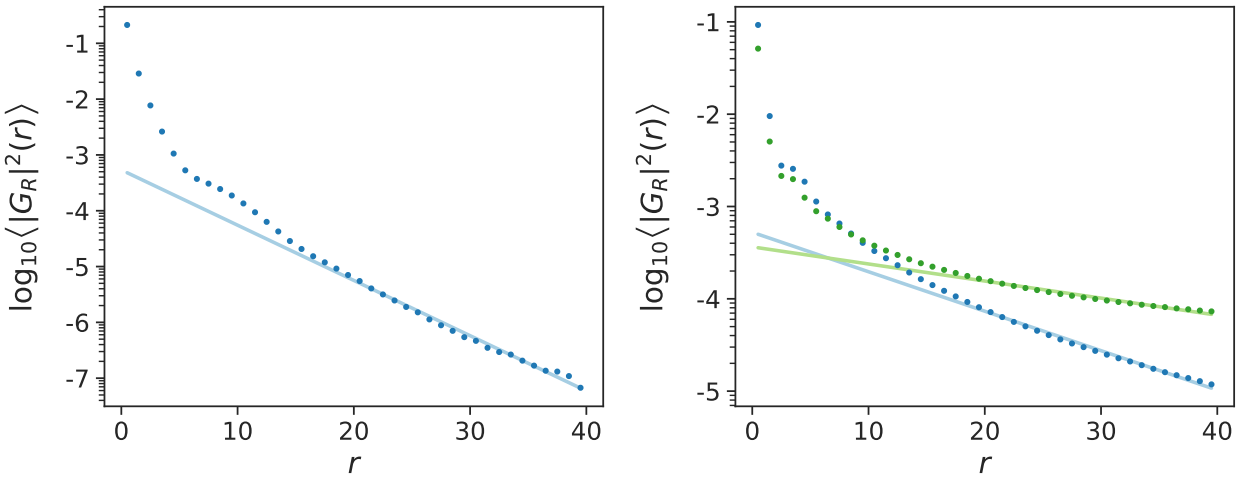

Figure 3.3: (a) $\langle|G^R_{\uparrow\uparrow}|^2\rangle_{dis}$ vs r for a localized state at $W = 13$ $\alpha = 0.3$. (b) $\langle|G^R_{\uparrow\uparrow}|^2\rangle_{dis}$ vs r for a delocalized state ($\alpha = 1.5$, in green) and an intermediate state ($\alpha = 1.0$, in blue) at $W = 13$.

the hamiltonian H in Eq 3.1 by drawing ϵ_i from a uniform distribution. This corresponds to a particular disorder realization drawn from an ensemble of possible disordered potentials. We diagonalize H using exact diagonalization to get the eigenfunctions ψ_n and eigenvalues E_n. We then construct $|G_R(i,\alpha;j,\beta)|^2$ using these eigenfunctions. $|G_R(i,\alpha;j,\beta)|^2$ is the square of the retarded Green's function at long times indicating the probability of a particle initially at r_j with spin β moving to r_i with spin α at long time,. We do this because we can extract the localization length from the $|G_R(i,\alpha;j,\beta)|^2$ values.

However, we can only draw conclusions from a quantity that has been averaged over the disorder ensemble. Therefore, we average $|G_R(i,\alpha;j,\beta)|^2$ over the 100 disorder realizations. The $|G_R(i,\alpha;j,\beta)|^2$ from each individual disorder realization does not possess translational invariance. However, the disorder averaged $\langle|G_R(i,\alpha;j,\beta)|^2\rangle_{dis}$ has translational invariance which allows us to construct the function $\langle|G_R|^2\rangle_{dis}(r)$. In the localized phase, we have $\langle|G^R_{\alpha\beta}|^2\rangle_{dis}(r) \propto e^{\frac{-2r}{\xi_{\alpha\beta}}}$ since the quantity represents the probability of a particle with spin β moving a distance r with spin α at long times. [2]. Therefore, the localization lengths can be inferred by fitting an exponential to the calculated quantities.

$$G_R(i,\alpha,t;j,\beta,0) = \sum_n \psi_n^*(i,\alpha)\psi_n(j,\beta)e^{-iE_nt}$$

$$\begin{aligned}\langle|G_R(i,\alpha,t;j,\beta,0)|^2\rangle_{dis} &= \left\langle \sum_{n,n'} \psi_n^*(i,\alpha)\psi_n(j,\beta)\psi_{n'}(i,\alpha)\psi_{n'}^*(j,\beta)e^{-i(E_n-E_{n'})t} \right\rangle_{dis} \\ &\approx \Bigg\langle \sum_n |\psi_n(i,\alpha)|^2|\psi_n(j,\beta)|^2 \\ &\quad + \sum_n \psi_n^*(i,\alpha)\psi_n(j,\beta)\psi_{\bar{n}}(i,\alpha)\psi_{\bar{n}}^*(j,\beta) \Bigg\rangle_{dis}\end{aligned} \tag{3.3}$$

Here we have taken the approximation that the crossed terms contribute negligibly when summed over as $(E_n - E_{n'})$ is nearly random, and thus, the sum over cross terms averages out to nearly zero. The only surviving terms are where $E_n = E_{n'}$. However, the system has time reversal symmetry and therefore, the spectrum exhibits a Kramer's degeneracy. This gives rise to the second term involving degenerate pairs of eigenfunctions $(\psi_n, \psi_{\bar{n}})$.

The exponentially decaying behaviour $\langle|G^R_{\alpha\beta}|^2\rangle_{dis}(r) \propto e^{\frac{-2r}{\xi_{\alpha\beta}}}$ is characteristic of the function at large r. At large r, the function becomes quite small and the number of data points also decrease as r increases. This expectation is illustrated in Figure 3.6b. Therefore, line fitting to $\langle|G^R_{\alpha\beta}|^2\rangle_{dis}(r)$ involves determining a range of r values over which the proportionality holds. Since our goal is to obtain an overall, coarse-grained picture of the phase diagram rather than finding exact critical exponents and characteristics of the transition, this method is sufficient.

As an example, we consider the phase point $(W = 13, \alpha = 0.3)$. The $\langle|G^R_{\uparrow\uparrow}|^2\rangle_{dis}(r)$ is plotted in Figure 3.3a. This point lies in the localized phase. We can see that the behaviour near $r = 0$ is markedly different as compared the behaviour at larger r. Moreover, for $r \sim L = 40$, we see a deviation from the linearity. We have ignored the data points beyond $r = L$ since $r \in [L, \sqrt{2}L]$ contains significantly lower number of data points than the rest of the graph. As such, this data matches our expectation and yields a small localization length. In contrast, the delocalized and intermediate state in Figure 3.3b do not decrease as fast as the localized state. They depict significantly lower slopes and the associated localization lengths are much larger. In fact, the associated localization length for the delocalized state

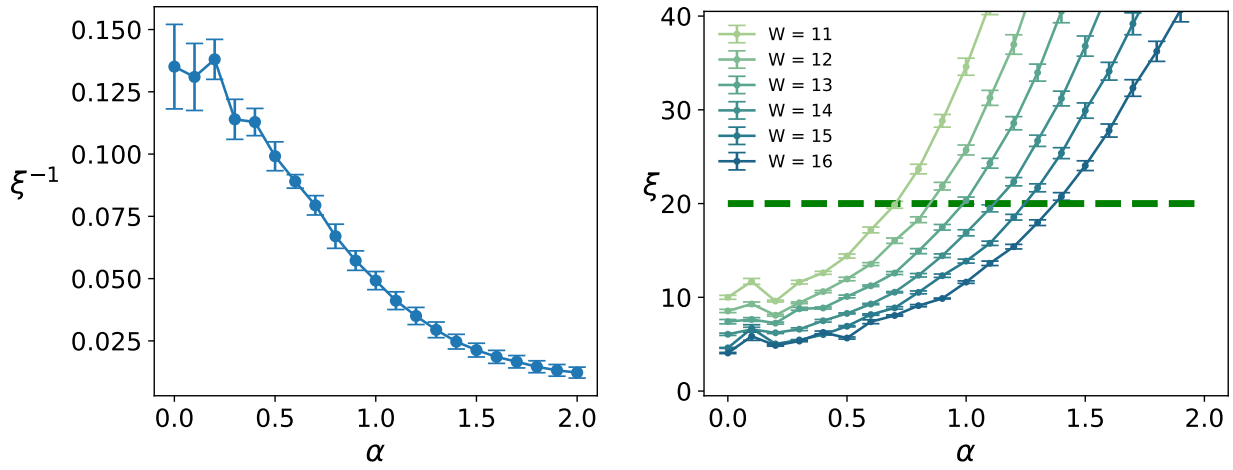

(a) (b)

Figure 3.4: (a) $\xi_{\uparrow\uparrow}^{-1}$ as a function of α for $W = 13$. (b) $\xi_{\uparrow\uparrow}$ for different disorder strengths W as a function of spin-orbit coupling strength α.

is much larger than the system size. The $\xi_{\uparrow\uparrow}$ for the intermediate state is around $O(L/2)$. If the localization length is larger than half the system size, then on a finite size system the state is effectively delocalized. Therefore, we set $r = L/2$ as a boundary for separating the localized and delocalized states. The dashed line in Figure 3.4b shows this distinction. In this manner, we now try to visualize the parameter space $W - \alpha$.

We considered a parameter space of $\alpha \in [0, 2]$ with spacing 0.1, $W \in [8, 18]$ with spacing 1 on a 40×40 lattice with open boundary conditions. The hamiltonian was diagonalized using exact diagonalization and the $|G_R|^2$ matrices were constructed. This matrix was averaged over 100 disorder realizations and then $\langle |G_R|^2 \rangle_{dis}(r)$ was constructed. The four functions $\ln \langle |G^R_{\uparrow\uparrow}|^2 \rangle_{dis}(r)$, $\ln \langle |G^R_{\uparrow\downarrow}|^2 \rangle (r)$, $\ln \langle |G^R_{\downarrow\uparrow}|^2 \rangle (r)$ and $\ln \langle |G^R_{\downarrow\downarrow}|^2 \rangle (r)$ were then fitted linearly in order to determine the corresponding localization lengths.

We see in Figure 3.5a and 3.5b that the localization lengths are small for low α and large W and the localization length increases as the disorder strength W is decreased and when the coupling strength α is increased. When the localization length is greater than half of the system size L, we consider the system to be delocalized.

The localization lengths increase as the spin-orbit coupling is increased and ξ diverges with increasing α. We can estimate that the system remains localized for ξ sufficiently lower than $L/2$ as beyond $L/2$, the wavefunction would have support over most of the finite size

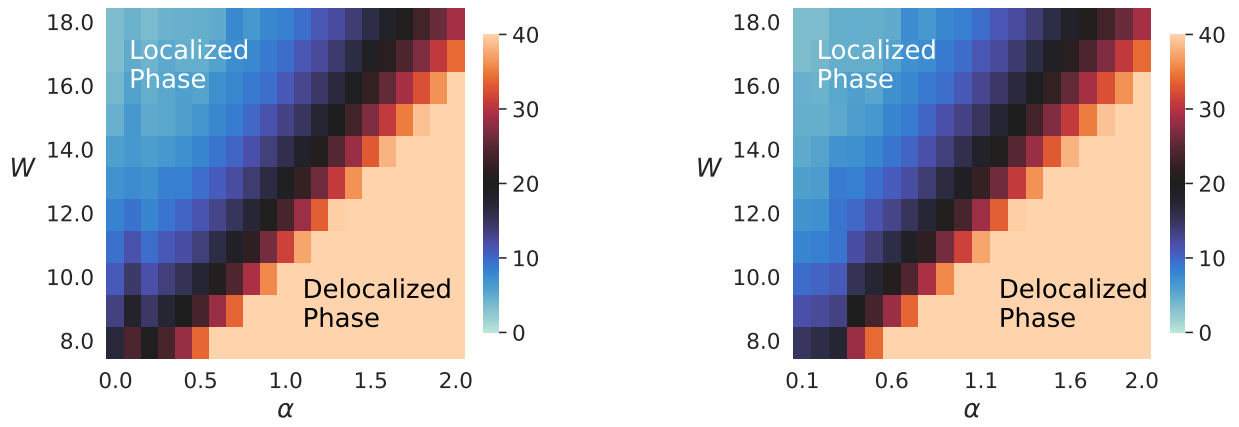

(a) (b)

Figure 3.5: (a) $\xi_{\uparrow\uparrow}$ over the parameter space for 40×40 lattice (b) $\xi_{\uparrow\downarrow}$ over the parameter space for 40×40 lattice

lattice. Overall, we see that the phase diagram does not look very different for the $\xi_{\uparrow\uparrow}$ and $\xi_{\uparrow\downarrow}$. This is exemplified in Figure 3.6a. We can interpret this as an indication that the spin-conserving hopping channels and the spin-flipping hopping channels have nearly the same localization length. Since there is no significant separation of scales at large r, we may conclude that the localization lengths associated with charge and spin densities will not be vastly different deep in the localized phase.

3.3 Problems in the Approach

There are a few issues with this approach of fitting exponentials to the Green's function squared. First, the range of r over which the fitting should take place is variable. The localization length extracted from the fit is sensitive to the range over which the fitting takes place. As a result, estimating the range correctly is crucial in order to obtain higher accuracy results. The proportionality $\langle |G^R_{\alpha\beta}|^2 \rangle_{dis}(r) \propto e^{\frac{-2r}{\xi_{\alpha\beta}}}$ is valid only for large r. For small values of r upto a microscopic length scale, the function shows a non-universal behaviour which does not match the exponential decay. This length scale is not available to us and varies significantly with the parameters. Second, since the simulations are done on finite system sizes, at large values of r, we have decreasing number of data points. We have set an upper bound of $r < L$ for fitting in order to combat this issue, however, this limits our r range.

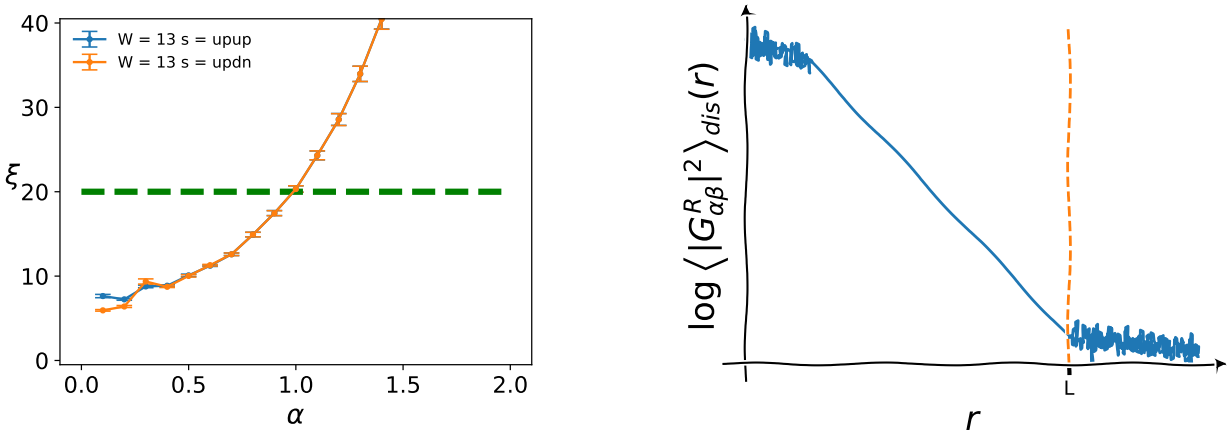

(a) (b)

Figure 3.6: (a) $\xi_{\uparrow\uparrow}$ (blue) vs $\xi_{\uparrow\downarrow}$ (orange) for $W = 13$ (b) Schematic plot of $\langle |G^R_{\alpha\beta}|^2 \rangle_{dis}(r)$.

Third, the function $\langle |G^R_{\alpha\beta}|^2 \rangle_{dis}(r)$ decreases rapidly with r. As a result, for large r the values are quite small. Therefore, the reliability of our calculations goes down since our resolution scale is $O(1/L^2)$.

These issues will continue to persist even if we go for a larger system size. Therefore, we must turn to a different, more reliable and simpler to measure quantity in order to characterize the localization effect. We choose spin and charge imbalance as our tools for doing this as described in the next chapter.

Chapter 4

Memory of Initial States

4.1 Thermalization and Memory Retention

In a typical large system, the state of the system at long times can be determined by just knowing the Hamiltonian. This is the prediction of statistical mechanics that states that the system will move into an equilibrium thermal state irrespective of the initial state at long times and this thermal state is determined solely by the system's energy spectrum. The process of thermalization thus involves the removal of the information about the initial state of the system in terms of quantities accessible through local observables. The information about the initial state, which is technically preserved by unitary evolution, is made inaccessible since it would require global operators to access them [26]. This involves the transport of local analogs of conserved macroscopic observables in order to achieve the thermal state. In contrast, certain quantum systems do not thermalize despite not being integrable. Systems that show Many Body Localization (MBL) fall under this category [26]. These systems do not evolve into a thermal state, instead they evolve into non-equilibrium states that are highly dependent on the initial state. As a result, they retain information about the initial state even at long times. This is because localization suppresses transport and hence impedes the thermalization process.

Recent experiments in 1D disordered, interacting systems have shown that such systems retain characteristics of their initial states while in the MBL phase [29, 21]. The systems in [29, 21] were initially prepared in a charge density wave with atoms occupying even sites

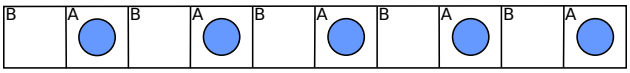

Figure 4.1: Schematic of initial state used in experiments [29, 21]

while the odd sites are empty as shown in Figure 4.1. Then the system was allowed to evolve in time. This spatial distribution of charge, with the atoms mostly on the A sublattice with B being mostly empty, is shown to be retained by the system in the MBL phase even at long times. Choi et al have done a similar experiment in 2D, but with the following initial state: charge present on the entire left half of the system with the right half being empty [10]. They observe a similar retention of the initial spatial distribution. The reason these experiments are interesting is that the Hamiltonian, after disorder averaging, is symmetric with respect to the A and B sublattices shown in Figure 4.1. The information discriminating between the two sublattices is only contained in the initial condition. Therefore, these results depict that the information about the initial state is accessible through a local observable. In a typical thermalizing system, the spatial charge distribution of initial state would get scrambled and homogenized through transport of the charge between regions of the system removing the information about the spatial charge distribution of the initial state. In the presence of localization, the particles mostly remain localized to their initial positions. As a result, the spatial distribution is retained even with time evolution and the transport mechanism of scrambling and homogenization is suppressed.

These experiments measured imbalance, an observable that quantifies the memory of the spatial pattern of the initial state. In these experiments, the particle imbalance is defined as $I = (N_{even} - N_{odd})/(N_{even} + N_{odd})$ where $N_{even/odd}$ represents the total charge density on even/odd sites. This particle imbalance measures whether the particles are still localized on the A sublattice or whether they have moved to the B sublattice. This is a relatively simpler observable than the elusive localization length which can't be directly observed. The experiments in [29, 21, 10] show that imbalance is nearly zero in the delocalized phase whereas it is non-zero and significant in the MBL phase.

While we do not consider interacting systems in our work here, these publications have inspired us to use imbalance as a measure of the localization in our system. Since non-interacting systems provide the baseline understanding that is needed in order to study systems with interactions, we have adopted the same tools for the non-interacting case in this work.

Chakraborty et al have shown numerically and analytically that the memory of initial states is retained in several interacting and non-interacting disordered systems of spinless fermions in 1D and 2D [8]. They have used Schwinger-Keldysh Field Theory to calculate imbalance in these systems. We build upon this work and extend the scheme to spin-1/2 fermions in the spin-orbit coupled 2D Anderson model.

With the addition of spin degrees of freedom, the system exhibits localization in spin and charge, therefore, we can compare and contrast the memory retention of the spin density and the charge density and their possible relations with each other. One can ask how the memory retention of spin and charge density are affected by the spin-orbit coupling strength. The spin and charge density also need not be independent of each other. It is possible that the memory retention of the initial charge configuration is dependent on the spin pattern in the initial configuration.

We show in this chapter that in the system of fermions in the 2D spin-orbit coupled Anderson model on a square lattice, the memory retention of the initial charge density and initial spin density both are high in the localized phase but they decreases to zero as we move into the delocalized phase. However, the two are not equal for all α. Interestingly, the memory retention of initial charge density and initial spin density show qualitatively different behaviours as a function of the spin-orbit coupling strength. In particular, the memory retention of the charge density is more robust with respect to increasing spin-orbit coupling for low values of α as compared to the memory retention of the spin density. However, at large spin-orbit coupling strengths, the memory retention of the initial spin density is higher than that of the initial charge density. The memory retention of the initial charge configuration is also shown to be independent of the spin pattern of the initial configuration.

4.2 Calculation of Imbalance

For the case of spinless fermions, Chakraborty et al [8] have discussed the persistence of memory of the initial state particle density configuration in the form of imbalances of particle density even at long times. We define imbalance $I_O^{AB}(t)$ for any quantity O over the sets A and B as

$$I_O^{AB}(t) = \frac{\sum_{i\in A} O_i(t) - \sum_{i\in B} O_i(t)}{\sum_{i\in A} O_i(0) - \sum_{i\in B} O_i(0)} \tag{4.1}$$

This definition of imbalance is a generalized version for any quantity O. Previous works have largely considered only the particle/charge density imbalance. However, since our systems have spin degrees of freedom which are significant, we have generalized the definition to include other quantities such as S_z, S_x and S_y. The normalization ensures that the imbalance at $t = 0$ is always unity. Since imbalance typically gets reduced by time evolution, $I_O^{AB} \in [-1, 1]$. This allows us to compare the memory retention of different quantities such as charge imbalance and S_z spin imbalance.

In systems that show localization, the imbalance present in the initial configuration has been shown to remain present at long times such as in the 1D and 2D Anderson model and in the 1D Aubry-Andre model. In 1D, the imbalance can also be calculated analytically for simple initial conditions. It can be calculated numerically for the other cases in 1D and 2D. Here we repeat the calculation for the spin-orbit coupling case since we expect the imbalance to remain persistent in the localized phase but not in the delocalized phase.

To calculate the imbalance, we need to first compute the charge and spin densities as well as the quantities S_x, S_y, S_z. In order to calculate these quantities, we use the Schwinger-Keldysh Field Theory. In this theory, the time evolution is expanded in terms of two contour integrals in $\rho(t) = U(t)\rho_0 U^\dagger(t)$, where ρ represents the density matrix of system state, the one for $U(t)$ and one for $U^\dagger(t)$ [19]. This gives rise to two fields ψ_+ and ψ_-. As a result, the theory has two independent one-particle Green's functions. The retarded Green's function $G_R(i, \alpha, t; j, \beta, t')$ corresponds to the amplitude that a particle at in state $|j, \beta\rangle$ at time t' would end up in the state $|i, \alpha\rangle$ at time $t(t > t')$ without any additional excitations. The other is the Keldysh Green's function $G_K(i, \alpha, t; j, \beta, t')$ which encapsulates information about the densities and currents in the system. It represents the actual amplitude that the particle at j, β at time t' propogates to i, α at time t.

We consider the fermions in 2D Anderson model with Rashba type spin-orbit coupling on a finite lattice of side length L and with open boundary conditions. To study the the system, we calculate the relations between G_K and the densities.

$$iG_K(\mu,t;\nu,t') = \langle [c_\mu(t)c_\nu^\dagger(t')]\rangle \tag{4.2}$$
$$iG_K(\mu,t;\nu,t) = \langle \delta_{\mu\nu} - 2c_\nu^\dagger\rangle$$

Here $\langle \ldots \rangle$ represents the expectation value. So we get

$$\begin{aligned}
\langle n_{i,\uparrow}\rangle &= \frac{1}{2}\left[1 - iG_K(i,\uparrow,t;i,\uparrow,t)\right] \\
\langle n_{i,\downarrow}\rangle &= \frac{1}{2}\left[1 - iG_K(i,\downarrow,t;i,\downarrow,t)\right] \\
\langle S_i^-\rangle &= \frac{-i}{2}G_K(i,\uparrow,t;i,\downarrow,t) \\
\langle S_i^+\rangle &= \frac{-i}{2}G_K(i,\downarrow,t;i,\uparrow,t)
\end{aligned} \tag{4.3}$$

From the work done by Chakraborty, Gorantla, Sensarma, we have a relation that allows us to compute G_K [9],

$$iG_K(i,\alpha,t;i,\beta,t) = \sum_{k,\gamma} G_R(i,\alpha,t;k,\gamma,0)G_R^*(i,\beta,t;k,\gamma,0)(1-2n_{k,\gamma}(0)) \tag{4.4}$$

We expand the $G_R G_R^*$ term into eigenfunctions of the hamiltonian,

$$G_R(i,\alpha;k,\gamma)G_R^*(i,\beta;k,\gamma) = \sum_{n,n'} \psi_n(i,\alpha)\psi_n^*(k,\gamma)\psi_{n'}^*(i,\beta)\psi_{n'}(k,\gamma)e^{-i(E_n-E_{n'})t}$$

Finally, the quantities are calculated at long times, therefore, we can take the limit $t \to \infty$. Since $E_n - E_{n'}$ is generally random, the summation consists of random phases leading to the term becoming negligibly small except when $E_n = E_{n'}$. This occurs for $n = n'$ and for any degeneracies in the system. Since our system has fermions and time-reversal symmetry, we see a double degeneracy for each energy level. However, there are no other

symmetries giving rise to degeneracies, so these are the only degeneracies in the spectrum. Defining $\psi_{\bar{n}}$ as the Kramer pair partner of ψ_n, we obtain,

$$G_R(i,\alpha;k,\gamma)G_R^*(i,\beta;k,\gamma) = \sum_n \psi_n(i,\alpha)\psi_n^*(i,\beta)|\psi_n(k,\gamma)|^2 + \sum_n \psi_n(i,\alpha)\psi_n^*(k,\gamma)\psi_{\bar{n}}^*(i,\beta)\psi_{\bar{n}}(k,\gamma) \tag{4.5}$$

The quantities $\langle n_\uparrow\rangle$, $\langle n_\downarrow\rangle$, $\langle \rho_{charge}\rangle$, $\langle S_x\rangle$, $\langle S_y\rangle$, $\langle S_z\rangle$ can all be expressed linearly in terms of the Keldysh Green's function G_K. Therefore, the imbalances can be written as

$$\begin{aligned} I^\infty &= \frac{1}{I_0}\left(\sum_{i\in A} G_K^\infty(i,\alpha;i,\beta) - \sum_{i\in B} G_K^\infty(i,\alpha;i,\beta)\right) \\ &= \sum_{i\in A}\sum_{k,\gamma} G_R^\infty(i,\alpha;k,\gamma)G_R^\infty(i,\beta;k,\gamma)^*(1-2n^0_{k,\gamma}) \\ &- \sum_{i\in B}\sum_{k,\gamma} G_R^\infty(i,\alpha;k,\gamma)G_R^\infty(i,\beta;k,\gamma)^*(1-2n^0_{k,\gamma}) \end{aligned} \tag{4.6}$$

We compute $G_R G_R^*$ for different initial spin and charge configurations on a 100×100 lattice and average it over 100 disorder realizations. After averaging, the quantity obtained is a translationally invariant quantity since the disorder is drawn from a uniform probability distribution. So the imbalances calculated are the disorder averages of the imbalances of the expectation values of quantities such as $n_\uparrow$, $n_\downarrow$, ρ_{charge}, S_z, S_x and S_y.

4.3 Results

In this section we present the results for the long time charge and spin imbalances in a 2D disordered spin-orbit coupled system. A key question which we would like to answer is whether the initial charge and spin patterns are equally robust to changes in spin-orbit coupling or whether one is more robust than the other.

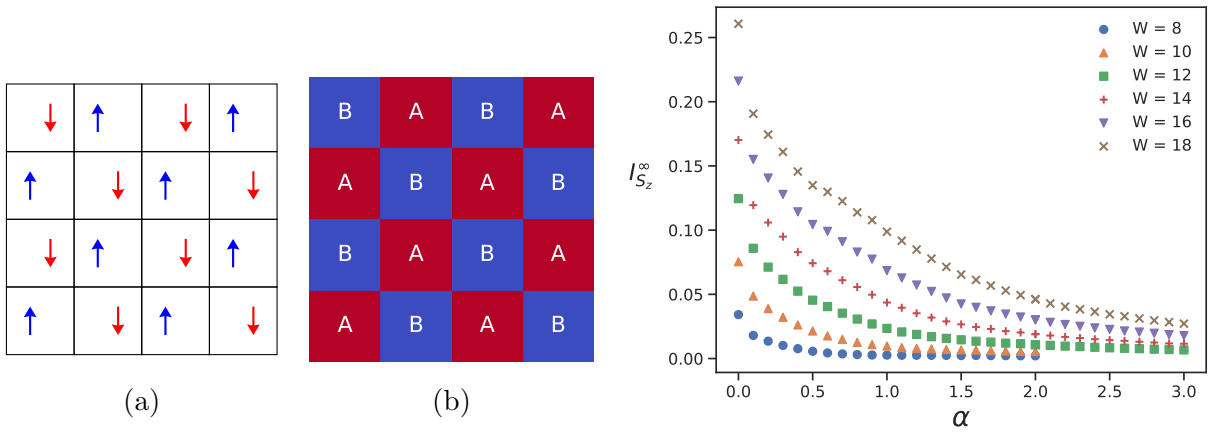

(a) (b) (c)

Figure 4.2: (a) represents the initial state which is anti-ferromagnetic (Néel state); (b) represents the sets the imbalance is calculated over: Set A in red, Set B in blue; (c) shows the S_z imbalance over a 100×100 lattice.

We first consider the dynamics of the system starting from a Néel state i.e. a checkerboard pattern with alternating sites, labelled as A and B sublattices, occupied by a single $\uparrow$ spin and a single $\downarrow$ spin. In this initial state, the imbalance in S_z between the A sublattice and B sublattice is 1. The long time S_z imbalance measures how much memory of the initial spin pattern is retained by the system.

The S_z spin imbalance is non-zero in the localized phase and decays to zero as we move to the delocalized phase. The imbalance decreases with increasing α and increases with increasing W. The imbalance near $\alpha = 0$ decays quite rapidly as the spin-orbit coupling is introduced. The decay to zero varies with (W, α) as we can see the the imbalance for $W = 8$ is nearly zero by time $\alpha = 1$ is reached, however, for $W = 18$, the imbalance is still non-zero for $\alpha = 3$.

We want to contrast this with the memory of charge density retained from a charge density wave. We start with a checkerboard pattern of charge density where A sublattice is doubly occupied and the B sublattice is singly occupied creating a charge density wave with (π, π) wavevector. However, this does not uniquely determine the spin configuration of B sublattice. Therefore, we consider two different cases: (i) The spins on the B sublattice are ordered ferromagnetically along one diagonal but anti-ferromagnetically along the perpendicular diagonal. (ii) The spins on B sublattice are assigned either $\uparrow$ or $\downarrow$ randomly with

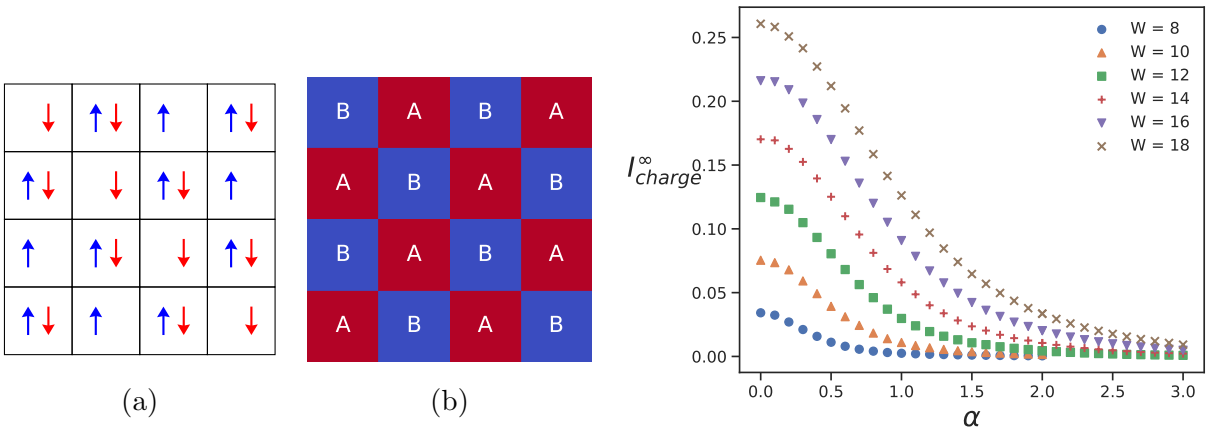

(a) (b) (c)

Figure 4.3: (a) represents the initial state which is which is a charge density wave with $S_z = 0$ on both the alternating sublattices; (b) represents the sets the imbalance is calculated over: Set A in red, Set B in blue; (c) shows the charge imbalance over a 100×100 lattice.

equal probability subject to the condition that there are an equal number of $\uparrow$ spins and $\downarrow$ spins. In this case, we average over these random spin configurations.

Figure 4.3c shows that the long time charge imbalance is finite in the absence of spin-orbit coupling. It decreases as the spin-orbit strength α increases and increases with increasing disorder strength W. Figure 4.4a also shows similar trends. In fact, the two are practically indistinguishable. This means that the presence of the spin pattern did not affect the behaviour of the charge imbalance. We can also note that the curvature of the imbalance curves is opposite of what the S_z spin imbalance in the previous case showed.

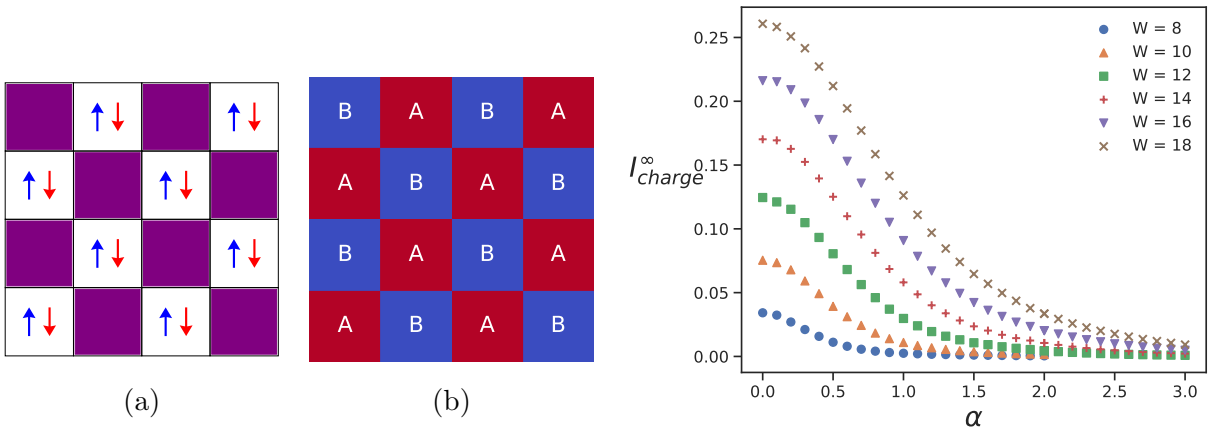

(a) (b) (c)

Figure 4.4: (a) represents the average over initial states that are charge density waves with the alternate sites (purple) being $|\uparrow\rangle$ or $|\downarrow\rangle$ with equal probability while keeping $\sum_B S_z = 0$ over all the purple sites in each state; (b) represents the sets the imbalance is calculated over: Set A in red, Set B in blue; (c) shows the average charge imbalance over a 100×100 lattice for all the random initial states.

4.4 Memory of Spin and Charge Imbalance

We compare the S_z spin imbalance for the spin density wave (Néel state) (Figure 4.2a) and the charge imbalance for the charge density wave (Figure 4.3a). Both of these show an imbalance of 1 for the initial state. The hamiltonian H in Eq 3.1 does not distinguish between the A and B sublattices (Figure 4.2b) across which the two imbalances are measured.

The results in Figure 4.5 show that the two types of imbalance show qualitatively different behaviour as the spin-orbit coupling strength is varied.

At $\alpha = 0$, both the charge and the spin imbalance are equal for all W. This case corresponds to the spinless fermion case. We only have a single localization length scale in this system and therefore, both the imbalances are equal. From [8], we can write the particle imbalance for the spinless fermion case as $I_p^{spinless} = f(\xi(W))$. Since each particle possesses a unit positive charge, $I_{charge} = f(\xi(W))$. Now, both the $\uparrow$ spin particles and the $\downarrow$ spin particles act as independent species of particles since there is no spin-orbit coupling. As a result, the S_z imbalance is given by $I_{S_z} = \left(\frac{1}{2}\right) I_{n_\uparrow} - \left(\frac{-1}{2}\right) I_{n_\downarrow}$. As the spin is conserved during hopping, the spin plays no role in the determination of imbalance, therefore $I_{n_\uparrow} = I_{n_\downarrow} =$

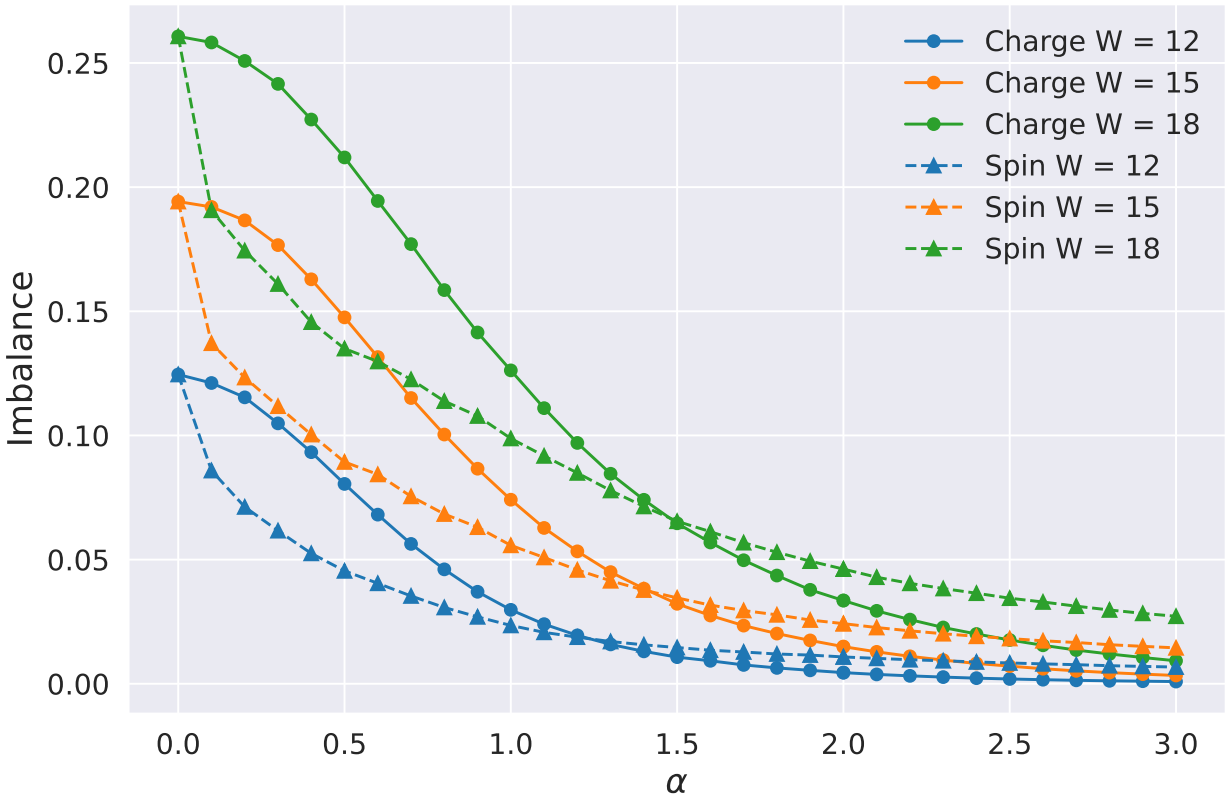

Figure 4.5: The charge imbalance (represented by circles) starting from the Charge Density Wave (Figure 4.3a) compared with the S_z imbalance (represented by triangles) starting from the Néel state (Figure 4.2a). The imbalances are equal for $\alpha = 0$, but the charge imbalance is more robust for small α while the S_z decreases rapidly on introduction of the spin-orbit coupling. On the other hand, S_z imbalance is slower to approach zero for larger α than the charge imbalance.

$f(\xi(W))$. So the charge imbalance from the charge density wave and spin imbalance from the Néel state are equal for $\alpha = 0$.

$$I_{charge}|_{\alpha=0}^{CDW} = I_{S_z}|_{\alpha=0}^{AFM} = f(\xi(W)) \tag{4.7}$$

At low α, the spin imbalance decays rapidly in comparison to the charge imbalance. The charge imbalance shows behaviour similar to an order parameter with a near quadratic decrease. The spin imbalance showcases a non-analytic behaviour similar to a $\alpha^{1/2}$ decrease. This $O(\alpha^2)$ vs $O(\alpha^{1/2})$ decrease is shown in Figure 4.6a and 4.6b.

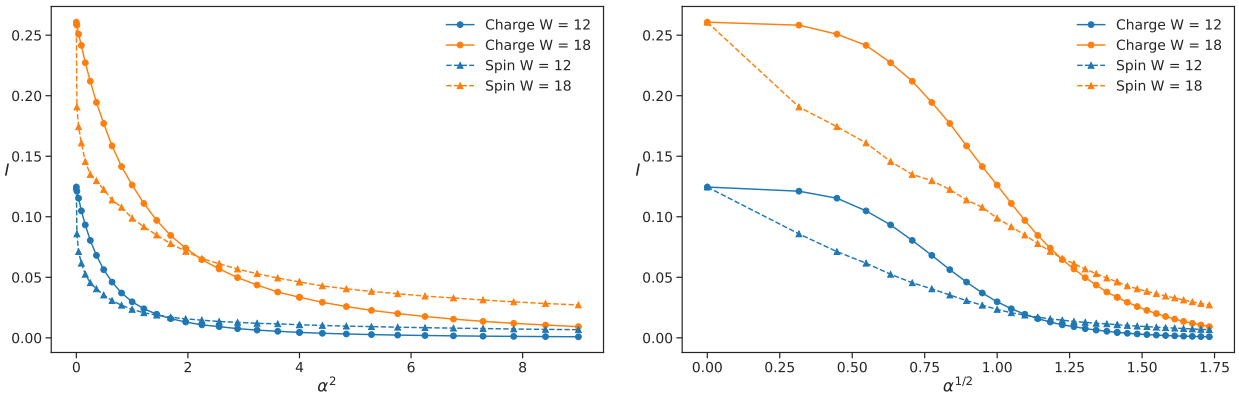

(a) (b)

Figure 4.6: (a) indicates the charge imbalance (represented by circles) and S_z imbalance (represented by triangles) for a charge and density wave resp. plotted wrt different powers of the spin-orbit coupling strength.

This behaviour of the spin imbalance seems non-analytic and is quite interesting. It is likely due to the availability of channels that do not conserve spins. This difference between charge and spin imbalance indicates the presence of different localization length scales involved in the problem, one associated with spin and the other with charge. These results need to be understood in greater detail from simpler models. We are currently working on these simpler models but that is beyond the scope of this thesis. The non-analyticity of the spin imbalance, in particular, presents an interesting theoretical challenge.

4.4.1 Possible Use Cases

The differences in response of the spin and charge imbalance to the addition of spin-orbit coupling represents a unique physical phenomena which could potentially be useful in a variety of different fields. Consider a 2D layer of spin-orbit coupled disordered in its insulating (localized) phase attached to a semiconductor or a metal strip which carries spin currents. By tuning the spin-orbit coupling strength in the insulator, one may be able to enable the spin degrees of freedom to thermalize and act as a thermal bath for the spin current while retaining the charge density distribution. This effect may allow the production of a controlled bath that regulates the degrees of freedom that the attached metal/semiconductor system is allowed to interact with. If we construct an initial state where the high energy charge and spin configurations are in the bulk of the insulator, the spin degrees of freedom would

delocalize faster and thus dominate the interaction with the attached system for low spin-orbit coupling. At high spin-orbit coupling both the charge and spin degrees of freedom would interact with the attached system.

The rapid decay in the retention of spin memory may also allow the creation of a spin-fuse. Consider a 2D layer of disordered spin-orbit coupled material in the localized phase. Under the normal circumstances, this strip would be insulating. However, if it was bombarded with a small number of heavy particles, the embedding of these heavy impurities could cause changes to the lattice symmetry locally that may enhance the effect of spin-orbit coupling. When bombarded with a critical number of heavy particles, the sample could start conducting enough to be measured. In this manner, it may act as as a fuse or a detector of certain heavy particles.

4.5 Additional Checks

We can also ask the question whether the dynamics depends on whether the charge imbalance is symmetric with respect to holes and particles. In order to check this, we consider an initial state similar to Figure 4.3a but with the double occupancy sites on sublattice A replaced by holes. The charge imbalance for such an hole initial state is nearly identical to that of the doublon initial state.

We can also ask the question whether the S_z spin imbalance in the Néel state is dependent on the absence of a background charge configuration. In order to check this, we consider the initial state from Figure 4.3a which we used to measure charge imbalance. Instead, we now measure the S_z spin imbalance but on A and B sublattices defined as in Figure 4.8c. This spin imbalance is nearly the same as the spin imbalance for the Néel state. Therefore, the presence of doubly occupied sites in the middle has not affected the spin imbalance.

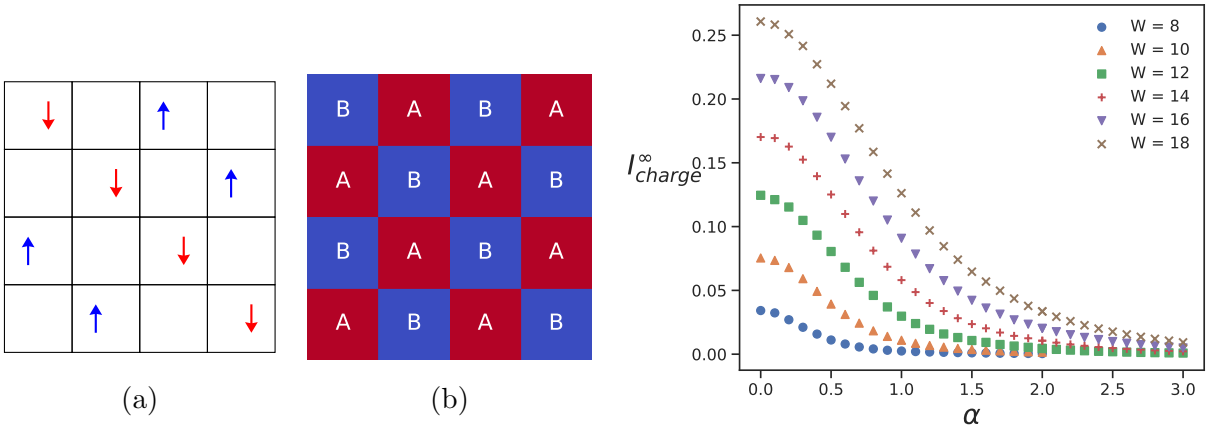

(a) (b) (c)

Figure 4.7: (a) represents the initial state which is a charge density wave that has holes instead of doublons as opposed to Figure 4.3a; (b) represents the sets the imbalance is calculated over: Set A in red, Set B in blue; (c) shows the charge imbalance over a 100×100 lattice.

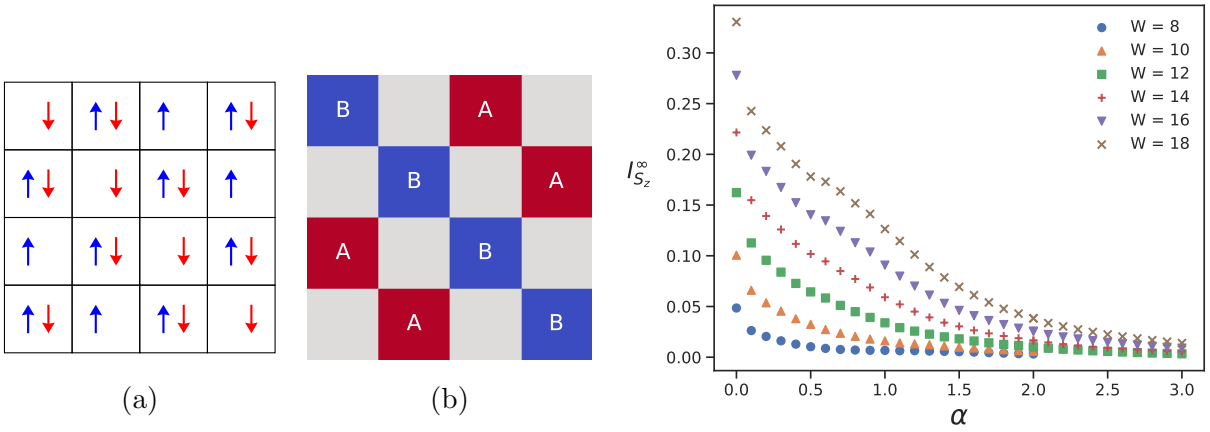

(a) (b) (c)

Figure 4.8: (a) represents the initial state which is which is a charge density wave with $S_z = 0$ on both the alternating sublattices; (b) represents the sets the imbalance is calculated over: Set A in red, Set B in blue, Ignored sites in grey; (c) shows the charge imbalance over a 100×100 lattice.

Chapter 5

Conclusion

The presence of spin-orbit coupling in a 2D Anderson model leads to a metal-insulator transition whose overall phase space has been determined. The system retains memory of its initial state in the localized phase. This has been quantified by the imbalance in charge density and S_z for different initial conditions. The charge imbalance and spin imbalance behave in qualitatively different ways and the charge density imbalance behaviour is not dependent on the presence or absence of a spin pattern in the initial condition. The memory retention of the initial charge density is more robust to the addition of spin-orbit coupling than the memory retention of the initial spin density. The spin imbalance seems to have non-analytic behaviour for low α.

5.1 Future Directions

The S_z spin imbalance decays rapidly with the introduction of a non-zero spin-orbit coupling strength. The behaviour of the this imbalance seems to be non-analytic. However, understanding this requires deeper analysis starting from simpler models. Establishing the origin and true nature of this apparent non-analyticity is a very interesting theoretical challenge. This may be in part due to the addition of channels accesible to the particle that do not conserve S_z whereas all the channels conserve charge.

The memory retention capacity of any system that exhibits storage capabilities is limited

by a range of frequencies which remain undissipated and accessible to the observer even after long times. This characteristic range of frequencies is particular to each information retention device and our system is no exception. We have considered charge density waves and spin density waves largely with a (π, π) wavevector. However, the imbalance may depend on the frequency of the density waves present in the initial state. This, however, requires a deeper analysis since our G_K expression derives from a Keldysh Field Theory result that is only valid when the initial state is a fock state and general spin spiral waves will not be fock states. These states would allow us to deal with larger number of imbalances in terms of S_x and S_y as well. Therefore, they may show interdependent S_x, S_y, S_z imbalances. The frequency dependence of the imbalance can also allow us to construct initial states that are relatively robust to the effect of spin-orbit coupling.

The difference in the qualitative behaviour between the charge and spin imbalance may allow one to construct devices that can tune the spin-orbit coupling in order to utilize the relative suppression of transport by the localization to allow the memory of either the charge configuration or the spin configuration to thermalize while the other is retained.

Appendix A

Calculating $G_R G_R^*$

This section is devoted to a discussion on how $G_R G_R^*$ was computed in an efficient manner. The construction of $G_R G_R^*$ from the eigenfunctions involves an $O(L^6)$ summation. This can be sped up by casting the computations involved as matrix multiplications. For each $G_R G_R^*$ calculation, there are two parts which contribute to the final matrix. The non-degenerate part is straightforward and similar to the spinless case in [8]. However, the presence of spinful fermions in the system means that there exists a double degeneracy which gives pairs of eigenvectors which have the same eigenvalue. These eigenvectors contribute significantly, therefore, we have a term involving these degenerate energies for each $G_R G_R^*$.

$$G_R(i,\alpha;k,\gamma)G_R^*(i,\beta;k,\gamma) = (A^{\alpha\beta}Z^T)_{i,2k+\gamma} + [C^{\alpha\beta}(C^{\gamma\gamma})^T]_{ik} + [C^{\beta\alpha}(C^{\gamma\gamma})^T]^*_{ik} \tag{A.1}$$

where we define

$$A^{\alpha\beta}_{in} = \psi_{n,2i+\alpha}\psi^*_{n,2i+\beta} \tag{A.2}$$

$$Z_{2k+\gamma,n} = |\psi_{2k+\gamma,n}|^2 \tag{A.3}$$

$$C^{\alpha\beta}_{ip} = \psi_{2p,2i+\alpha}\psi^*_{2p+1,2i+\beta} \tag{A.4}$$

This is convenient since the diagonalization procedure used will often return the eigenvectors in the form $\psi_n(i,\sigma) = \psi_{n,2i+\sigma}$. So indices used are n running over 0 to $2L^2-1$ while i,p,k run over 0 to L^2-1.

These $G_R(i,\alpha;k,\gamma)G_R^*(i,\beta;k,\gamma)$ matrices are not symmetric and are, in general, complex. Since $G_R(i,\alpha;k,\gamma)G_R^*(i,\beta;k,\gamma) = \mathbb{G}^{\alpha\beta}_{i,2k+\gamma}$ is a non-square matrix, there are no hermitian or symmetric matrix simplifications in the computations or storage. However, we do have $G_R(i,\alpha;k,\gamma)G_R^*(i,\beta;k,\gamma) = [G_R(i,\beta;k,\gamma)G_R^*(i,\alpha;k,\gamma)]^*$. This allows us to reduce the number of calculations of complex matrix multiplications.

Bibliography

[1] E. Abrahams et al. "Scaling Theory of Localization: Absence of Quantum Diffusion in Two Dimensions". In: *Phys. Rev. Lett.* 42.10 (Mar. 5, 1979), pp. 673–676.

[2] P. W. Anderson. "Absence of Diffusion in Certain Random Lattices". In: *Phys. Rev.* 109.5 (Mar. 1, 1958), pp. 1492–1505.

[3] T. Ando. "Numerical Study of Symmetry Effects on Localization in Two Dimensions". In: *Phys. Rev. B* 40.8 (Sept. 15, 1989), pp. 5325–5339.

[4] Yoichi Asada, Keith Slevin, and Tomi Ohtsuki. "Anderson Transition in Two-Dimensional Systems with Spin-Orbit Coupling". In: *Phys. Rev. Lett.* 89.25 (Dec. 3, 2002), p. 256601.

[5] Juliette Billy et al. "Direct Observation of Anderson Localization of Matter Waves in a Controlled Disorder". In: *Nature* 453.7197 (7197 June 2008), pp. 891–894.

[6] Robin Bläsing et al. "Magnetic Racetrack Memory: From Physics to the Cusp of Applications Within a Decade". In: *Proceedings of the IEEE* 108.8 (Aug. 2020), pp. 1303–1321.

[7] A. A. Chabanov, M. Stoytchev, and A. Z. Genack. "Statistical Signatures of Photon Localization". In: *Nature* 404.6780 (6780 Apr. 2000), pp. 850–853.

[8] Ahana Chakraborty, Pranay Gorantla, and Rajdeep Sensarma. "Memories of Initial States and Density Imbalance in the Dynamics of Noninteracting and Interacting Disordered Systems". In: *Phys. Rev. B* 102.22 (Dec. 21, 2020), p. 224306.

[9] Ahana Chakraborty, Pranay Gorantla, and Rajdeep Sensarma. "Non-Equilibrium Field Theory for Dynamics Starting from Arbitrary Athermal Initial Conditions". In: *Phys. Rev. B* 99.5 (Feb. 19, 2019), p. 054306.

[10] Jae-yoon Choi et al. "Exploring the Many-Body Localization Transition in Two Dimensions". In: *Science* 352.6293 (June 24, 2016), pp. 1547–1552.

[11] Tanmoy Das and A. V. Balatsky. "Engineering Three-Dimensional Topological Insulators in Rashba-type Spin-Orbit Coupled Heterostructures". In: *Nat Commun* 4.1 (1 June 6, 2013), p. 1972.

[12] J. T. Edwards and D. J. Thouless. "Numerical Studies of Localization in Disordered Systems". In: *J. Phys. C: Solid State Phys.* 5.8 (Apr. 1972), pp. 807–820.

[13] S. N. Evangelou and T. Ziman. "The Anderson Transition in Two Dimensions in the Presence of Spin-Orbit Coupling". In: *J. Phys. C: Solid State Phys.* 20.13 (May 1987), pp. L235–L240.

[14] Ulrich Fastenrath. "Localization Properties of 2D Systems with Spin-Orbit Coupling: New Numerical Results". In: *Physica A: Statistical Mechanics and its Applications* 189.1 (Oct. 15, 1992), pp. 27–42.

[15] Victor Galitski and Ian B. Spielman. "Spin–Orbit Coupling in Quantum Gases". In: *Nature* 494.7435 (7435 Feb. 2013), pp. 49–54.

[16] M. Z. Hasan and C. L. Kane. "Colloquium: Topological Insulators". In: *Rev. Mod. Phys.* 82.4 (Nov. 8, 2010), pp. 3045–3067.

[17] Shinobu Hikami, Anatoly I. Larkin, and Yosuke Nagaoka. "Spin-Orbit Interaction and Magnetoresistance in the Two Dimensional Random System". In: *Progress of Theoretical Physics* 63.2 (Feb. 1, 1980), pp. 707–710.

[18] Lianghui Huang et al. "Experimental Realization of Two-Dimensional Synthetic Spin–Orbit Coupling in Ultracold Fermi Gases". In: *Nature Phys* 12.6 (6 June 2016), pp. 540–544.

[19] Alex Kamenev. *Field Theory of Non-Equilibrium Systems*. Cambridge: Cambridge University Press, 2011.

[20] Y.-J. Lin, K. Jiménez-García, and I. B. Spielman. "Spin–Orbit-Coupled Bose–Einstein Condensates". In: *Nature* 471.7336 (7336 Mar. 2011), pp. 83–86.

[21] Henrik P. Lüschen et al. "Signatures of Many-Body Localization in a Controlled Open Quantum System". In: *Phys. Rev. X* 7.1 (Mar. 21, 2017), p. 011034.

[22] Roman M. Lutchyn, Jay D. Sau, and S. Das Sarma. "Majorana Fermions and a Topological Phase Transition in Semiconductor-Superconductor Heterostructures". In: *Phys. Rev. Lett.* 105.7 (Aug. 13, 2010), p. 077001.

[23] A. Manchon et al. "New Perspectives for Rashba Spin–Orbit Coupling". In: *Nature Mater* 14.9 (9 Sept. 2015), pp. 871–882.

[24] F. L. Moore et al. “Atom Optics Realization of the Quantum $\ensuremath{\delta}$-Kicked Rotor”. In: *Phys. Rev. Lett.* 75.25 (Dec. 18, 1995), pp. 4598–4601.

[25] Naoto Nagaosa and Yoshinori Tokura. “Topological Properties and Dynamics of Magnetic Skyrmions”. In: *Nature Nanotech* 8.12 (12 Dec. 2013), pp. 899–911.

[26] Rahul Nandkishore and David A. Huse. “Many-Body Localization and Thermalization in Quantum Statistical Mechanics”. In: *Annual Review of Condensed Matter Physics* 6.1 (2015), pp. 15–38.

[27] Giuliano Orso. “Anderson Transition of Cold Atoms with Synthetic Spin-Orbit Coupling in Two-Dimensional Speckle Potentials”. In: *Phys. Rev. Lett.* 118.10 (Mar. 6, 2017), p. 105301.

[28] Giacomo Roati et al. “Anderson Localization of a Non-Interacting Bose–Einstein Condensate”. In: *Nature* 453.7197 (7197 June 2008), pp. 895–898.

[29] Michael Schreiber et al. “Observation of Many-Body Localization of Interacting Fermions in a Quasirandom Optical Lattice”. In: *Science* 349.6250 (Aug. 21, 2015), pp. 842–845.

[30] Tal Schwartz et al. “Transport and Anderson Localization in Disordered Two-Dimensional Photonic Lattices”. In: *Nature* 446.7131 (7131 Mar. 2007), pp. 52–55.

[31] K. V. Shanavas, Z. S. Popović, and S. Satpathy. “Theoretical Model for Rashba Spin-Orbit Interaction in d Electrons”. In: *Phys. Rev. B* 90.16 (Oct. 7, 2014), p. 165108.

[32] Martin Störzer et al. “Observation of the Critical Regime Near Anderson Localization of Light”. In: *Phys. Rev. Lett.* 96.6 (Feb. 15, 2006), p. 063904.

[33] D. J. Thouless. “Localization Distance and Mean Free Path in One-Dimensional Disordered Systems”. In: *J. Phys. C: Solid State Phys.* 6.3 (Feb. 1973), pp. L49–L51.

[34] Diederik S. Wiersma et al. “Localization of Light in a Disordered Medium”. In: *Nature* 390.6661 (6661 Dec. 1997), pp. 671–673.

[35] Lu Zhou, Han Pu, and Weiping Zhang. “Anderson Localization of Cold Atomic Gases with Effective Spin-Orbit Interaction in a Quasiperiodic Optical Lattice”. In: *Phys. Rev. A* 87.2 (Feb. 25, 2013), p. 023625.

[36] Igor Žutić, Jaroslav Fabian, and S. Das Sarma. “Spintronics: Fundamentals and Applications”. In: *Rev. Mod. Phys.* 76.2 (Apr. 23, 2004), pp. 323–410.